Shahrood University of Technology

Journal of Mining and Environment (JME)

Journal homepage: www.jme.shahroodut.ac.ir

Iranian Society of Mining Engineering (IRSME)

Application of fractal models for determining distribution pattern of REEs and Lithium in North Kochakali coal deposit, Tabas

Mojtaba Bazargani Golshan[1], Mehran Arian[1]*, Peyman Afzal[2], Lili Daneshvar Saein[3], and Mohsen Aleali[4]

1. Department of Earth Sciences., Science and Research Branch, Islamic Azad University, Tehran, Iran
2. Department of Petroleum and Mining Engineering., South Tehran Branch, Islamic Azad University, Tehran, Iran
3. Department of Geology., Payame Noor University, PO Box: 19395-3697, Tehran, Iran
4. Department of Earth Sciences., Science and Research Branch, Islamic Azad University, Tehran, Iran

Article Info

Received 9 November 2024

Received in Revised form 29 November 2024

Accepted 12 December 2024

Published online 12 December 2024

DOI: 10.22044/jme.2024.15323.2938

Keywords

Concentration-Area fractal model

Concentration-Number fractal model

REEs

Lithium

North Kochakali

Abstract

The purpose of this research is application of the Concentration-Number and Concentration-Area fractal models for determining the distribution pattern of REEs and lithium in mining area of the North Kochakali coal deposit. According to the Concentration-Area and Concentration-Number fractal graphs, four different geochemical groups were obtained for REEs and lithium in the mining area of North Kochakali coal deposit. The comparison of the threshold values and the models obtained based on the Concentration-Area and Concentration-Number fractal models indicate that the Concentration-Area Fractal model has performed better in determining different geochemical groups and separating anomalies from the background for REEs and lithium in North Kochakali coal deposit. Based on the fractal models in the mining area, the southeastern and western parts have the highest concentrations of REEs and the northeastern parts have the highest concentrations of lithium. These parts should be considered in mining operations due to their higher economic value. The locations of the REEs anomalies are consistent with the location of right-lateral faults with a normal component, since these faults are young and have operated after the formation of coal seams, so the mineralization of REEs in North Kochakali coal deposit is epigenetic.

1. Introduction

One of the main issues when extracting and exploiting mines is preparing zoning maps to determine the areas with elements of high economic value and the areas with low economic value [1, 2]. These zoning maps in addition to showing the distribution of elements in the mining area, have a very important role in the planning and exploitation of mines [3]. For the evolution of low-carbon, renewable energy technologies, REEs are crucial [4]. Due to their physical properties, REEs are used in military, new energy development, technology, metallurgy, modern agriculture, and other fields [5]. There are critical elements, including Li, Ga, Ge, U, REY, Zr, Nb, Sc, V, Au, Ag, and Re, as well as Al and Mg in coal, so coal can be an important source of these elements [6-9]. Due to the low volatility of these elements, they are preserved in coal ash during the combustion process [10, 11]. In general, REEs (Rare earth elements) are divided into two groups: light rare earth elements (LREEs) and heavy rare earth elements (HREEs). Some types of coal have more enrichment of LREEs than HREEs, while some other HREEs show a better enrichment, this difference can be caused by the ancient environment of coal formation and geological location [12, 13, 10, 14]. Research shows that HREEs have higher affinity with coal organic matter [15, 16]. Finding lithium reserves in coal can greatly increase value of coal resources [17,

Corresponding author: mehranarian@yahoo.com (M. Arian)

18] and partially compensate for the lack of lithium in industrial cases [19]. Various researchers conducted studies on the origin of lithium in coal. [17] concluded that clay minerals (illite, kaolinite, smectite, etc.) in coal are the main source of lithium. [20, 21] considered geological factors as the main cause of enrichment of REEs in coal, in general, they proposed 5 factors for the genesis of REEs in coal, including: magmatic and hydrothermal processes, faulting, source rock, volcanic, groundwater and seawater, among these factors, a specific geological factor prevails over other factors in the enrichment of REEs. [22] and [23] suggested 2 main sources for lithium 1- The weathering of volcanic bedrock with lithium upstream in the areas where the amount of precipitation is high, then surface and ground water with lithium accumulate in the basin where the rate of evaporation is higher than the precipitation, which causes concentration and accumulation of lithium 2- Direct entry of hydrothermal fluids with lithium into the basin by the faults in the basin floor. Geological processes such as faulting, in addition to causing the displacement of coal seams, by predisposing the passage of fluids and also intrusive igneous masses, lead to enrichment and increase in the concentration of an element and set of elements.

Identifying the areas showing the enrichment of specific element or elements indicates real mineralization zone, and in geochemical exploration the identification of mineralization zones and separation anomalies from the background are fundamental issues [24-28]. Fractal/multifractal models, developed by [29] are used in various branches of earth sciences [30] such as: geochemistry [29, 31-35] geophysics [36-41], structural geology [42-45], and remote sensing [46, 47].

In geochemical processes fractal dimensions correspond to differences in physical characteristics such as hydrothermal fluid, structural feature, alteration, and so on [48]. The presence of geochemical anomalies increases the fractal dimension of geochemical variables, and based on differences in fractal dimensions, various stages of element distribution can be separated [49].

Fractal methods such as Concentration – Area [50], Concentration – Volume [49], Power spectrum-Area [51], Concentration – Perimeter [50] and Concentration – Number [29, 52] have been widely used in order to separate anomalies from the background. In Concentration-Number (C-N) fractal model separation anomaly is based on the inverse relationship between cumulative frequency of each concentration and higher concentrations [26, 52], but Concentration-Area (C-A) fractal model is based on inverse relationship between the element concentrations and the area occupied by them [50, 53].

In this research, 28 samples were taken from target seams in mining area of North Kochakali coal deposit. After analyzing and determining the concentrations of REEs and lithium, Concentration-Number and Concentration-Area fractal models were used in order to identify anomalous parts (high-concentration areas) and distribution pattern of REEs and lithium in North Kochakali coal deposit. These parts have a higher economic value and should be taken into account during mining operations. Finally, two fractal models were compared in terms of applications in separation anomalies from the background.

2. Geological Setting

2.1. Regional geology

North Kochakali coal deposit is located in the northern part of the Tabas block in the Central Iranian Micro-continent (CIM). With the opening of the Neotethys ocean, the CIM separated from the Gondwana supercontinent during the Permian and collided with the Eurasian plate as a result of the closure of the Paleotethys ocean [54, 55]. CIM consists of three structural blocks including: Tabas, Lut and Yazd, which today can be identified from east to west by faults with a north-south trend (Nayband and Naini faults). However, the relationship of these three blocks during the Jurassic period is still debated due to the clockwise rotation of the CIM in the Triassic, but this rotation probably happened in the post-Jurassic period [56, 57]. Tabas coal field with an area of 45,000 km^2 is located 80 to 200 kilometers south and southwest of Tabas. The Nayband fault in the east and the Naini and Kalmard faults are the enclosing faults of this basin. The coal reserve discovered in the Tabas coal zone is estimated at about 3 billion tons. North Kochakali area is located in South Khorasan province, about 75 km southwest of Tabas city (70 km west of Parvadeh coal mine) (Figure 1). In the North Kochakali and Mazinu mines, coal-bearing sediments are located inside Hojedk Formation, which has deltaic facies with a series of sandstone sediments, green shales, coaly shales, and coal seams in this Formation have created huge reserves of coal both in the north and in the south of Tabas block. Coal in North Kochakali and Mazinu mines are thermal type and anthracite to semi-anthracite.

In the North Kochakali area, in the northern part of Tabas block, the Badamu Formation is located at the lower boundary of the Hojedk Formation and the Parvadeh Formation is located at the upper boundary of the Hojedk Formation [58]. The Hojedk coal Formation was deposited in a back-arc basin related to the Neotethys subduction during the Late Triassic-Middle Jurassic [59]. Normal faults at the bottom of the back-arc basin have increased its subsidence rate. The intrusive igneous masses were injected into the coal deposit through the normal faults of the basin floor during the Paleogene [60]. During the Neogene and Quaternary, with the closure of the back-arc basin and the collision of the Arabian Plate with the Cimmerian Plate, the stress changes from tensile to compressive and the normal fault changes to the reverse strike-slip fault such a situation leads to the folding and uplift of the Hojedk Formation.

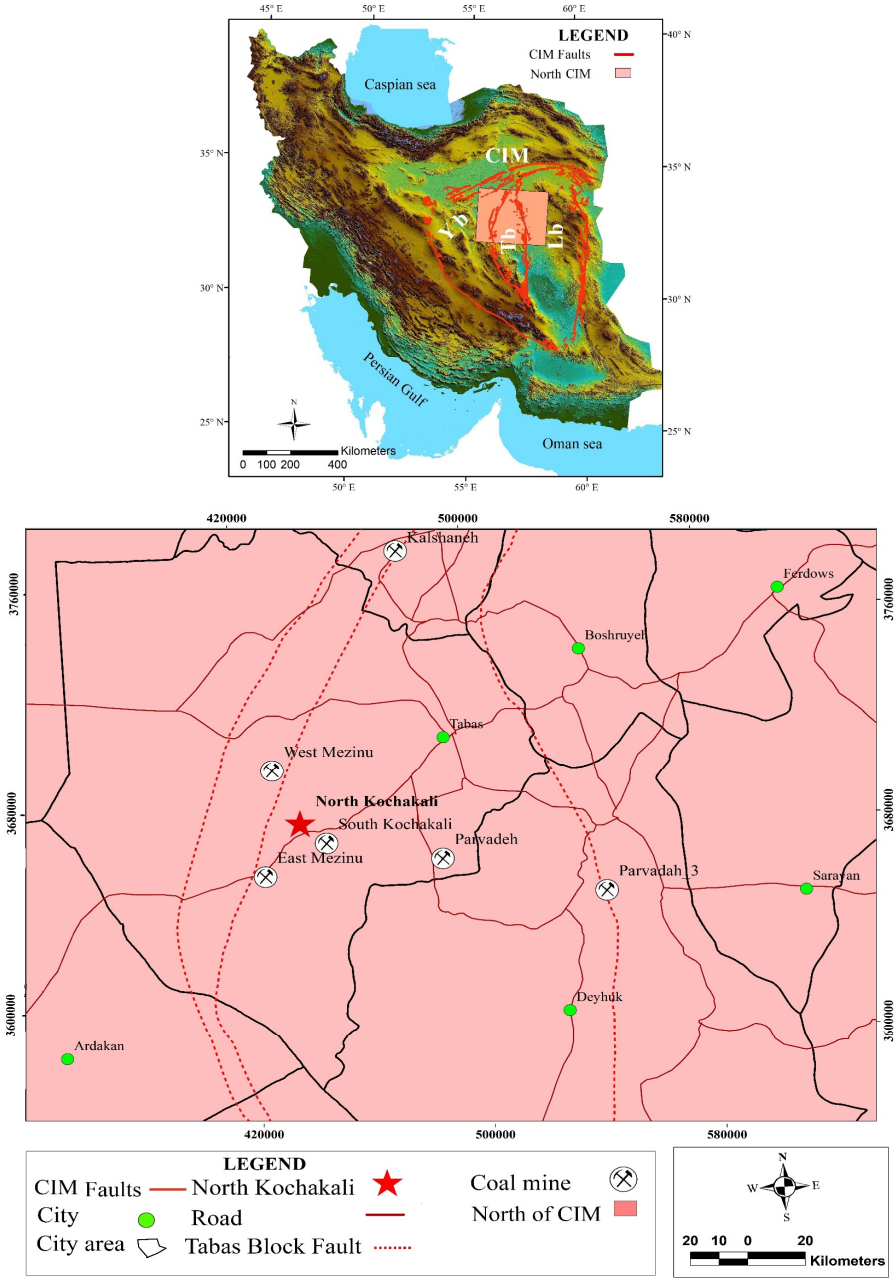

Figure 1. a-Geological Setting of Lut, Tabas and Yazd blocks. Lb: Lut block; Yb: Yazd block; Tb: Tabas block; CIM: Central Iranian Microcontinent, b- Geographic location of the North Kochakali, Parvadeh and Mazinu coal mines (modified after [61]).

In general, there are 4 outcrops of Formations in the North Kochakali area, which include: Ab Haji (J_{ab}) and Badamu (J_{bd}) Formations with Lower Jurassic age and Hojedk (J_h), Parvadeh (J_p) and Baghamshah (J_{bg}) Formations with Middle Jurassic age. Four main structures (two synclines and two anticlines) have been identified in the North Kochakali area. In the Anticline structures Ab-Haji Formation, the core and Badamu Formation form a part of the limb of these structures while in the syncline structures, the Baghamshah Formation is located in the core and the Parvadeh Formation is located in the limb of these structures (Figure 2). Field surveys and satellite images show that these structures have been greatly affected by faulting and their axial trend has changed, but in general, the axial trend of these structures is north-south. (Figure 3).

Figure 2. Syncline structure in the southwest of the North Kochakali coal deposit and the outcrops of the Hojedk, Parvadeh and Baghamshah Formations and the boundary between them. J_h: Hojedk Formation; J_p: Parvadeh Formation; J_{bg}: Baghamshah Formation.

2.2. Structural geology

Three types of faults have been identified in the North Kochakali area, which include thrust faults, left-lateral faults with reverse component, and right-lateral faults with normal component. In order to accurately detect the fault mechanism, sections of the target seams were used in the direction of the drilled boreholes. For this purpose, three vertical sections in the west-east direction at the crossing of thrust faults and a section in the north-south direction at the crossing of left-lateral and right-lateral faults were designed (Figure 4). Section C-C' indicate two thrust faults in the mining area, which are named as F1 and F2 (Figure 7). Sections A-A' between two boreholes 108 and 136, which are located at a distance of 600 meters from each other, the target seams have displacement in depth by about 200 meters (Figure 5). Also in section B-B, the target seams between two boreholes 104 and 130 have displacement more than 200 meters, which is the result of F1 fault (Figure 6). Section C-C' Section C shows that in addition to fault F1, there is another fault with less displacement (between two boreholes 156 and 123) in the area, which is named as fault F2 (Figure 7). These two faults (F1 and F2) have a slope towards each other and have created a Pop-up structure in the mining area of North Kochakali (Figure 8). Also, in order to detect the function of right-lateral and left-lateral faults a section in the north-south direction (section D-D) which is crossed between 111, 115, 109, 117 and 102 boreholes were designed. This section shows that these strike-slip faults have a slope-slip component (Figure 9). In North Kochakali area direction of greatest stress (σ_1) is east-west and direction of least stress (σ_3) is north-south, which can be justified according to the direction of the structures of the North Kochakali area (synclines and anticlines). As a result, left-lateral faults that have a trend from northwest to southeast have a reverse component, and right-lateral faults that have a trend from northeast to southwest have a normal component. The Sections show that the two thrust faults in the North kochakali area have been strongly displaced by strike-slip faults with normal and reverse components, which is a sign that the strike-slip faults with normal and reverse components are younger than the thrust faults in the North kochakali area. Also, the displacement of coal seams by faults indicates that the faults in this area have operated after the formation of coal seams.

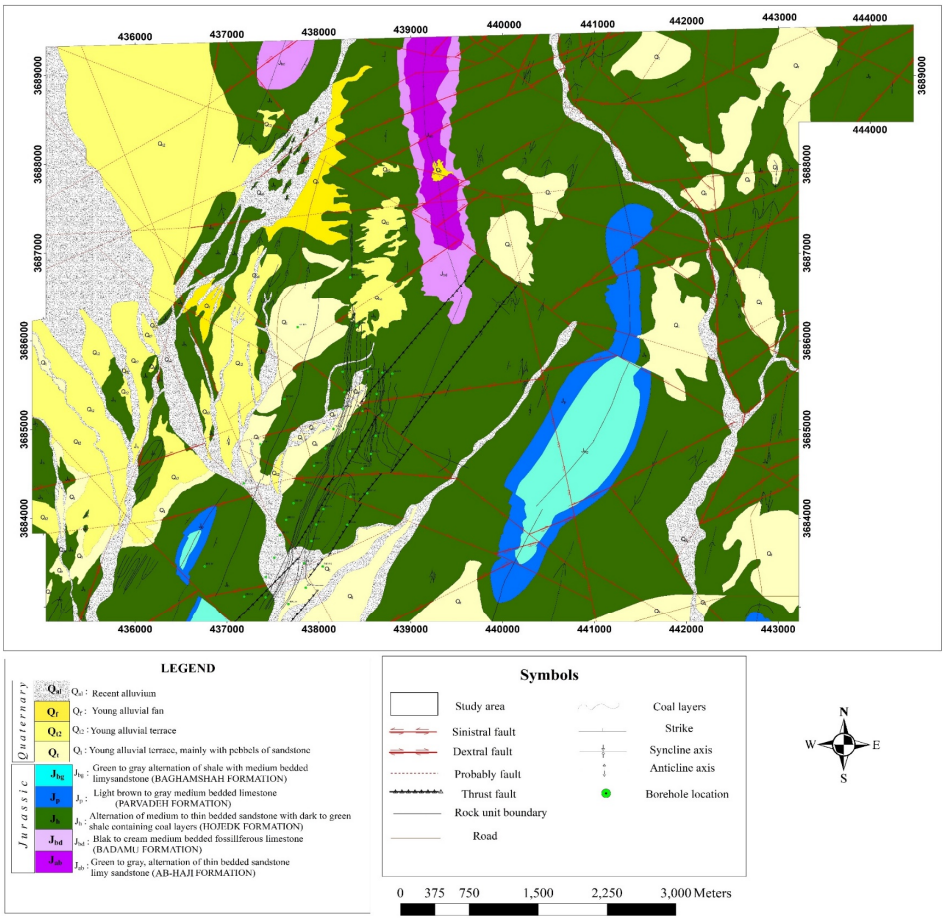

Figure3. Geological map of North Kochakali coal deposit. J_{ab}: Ab-Haji Formation; J_{bd}: Badamu Formation; J_h: Hojedk Formation, J_p: Parvadeh Formation; J_{bg}: Baghamshah Formation.

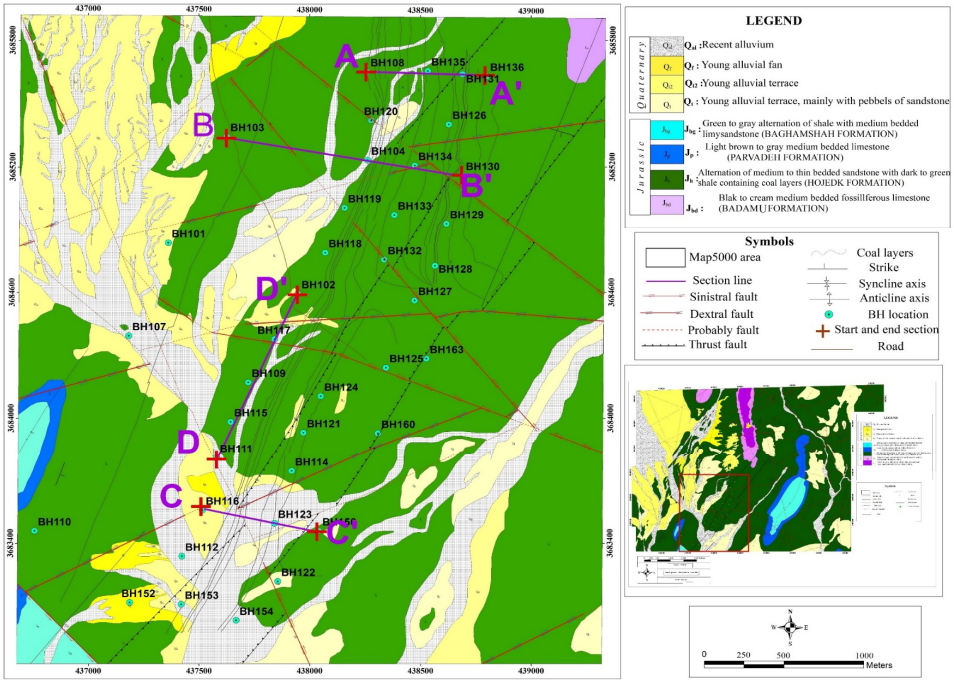

Figure 4. 1:5000 map of North Kochakali coal deposit with section lines

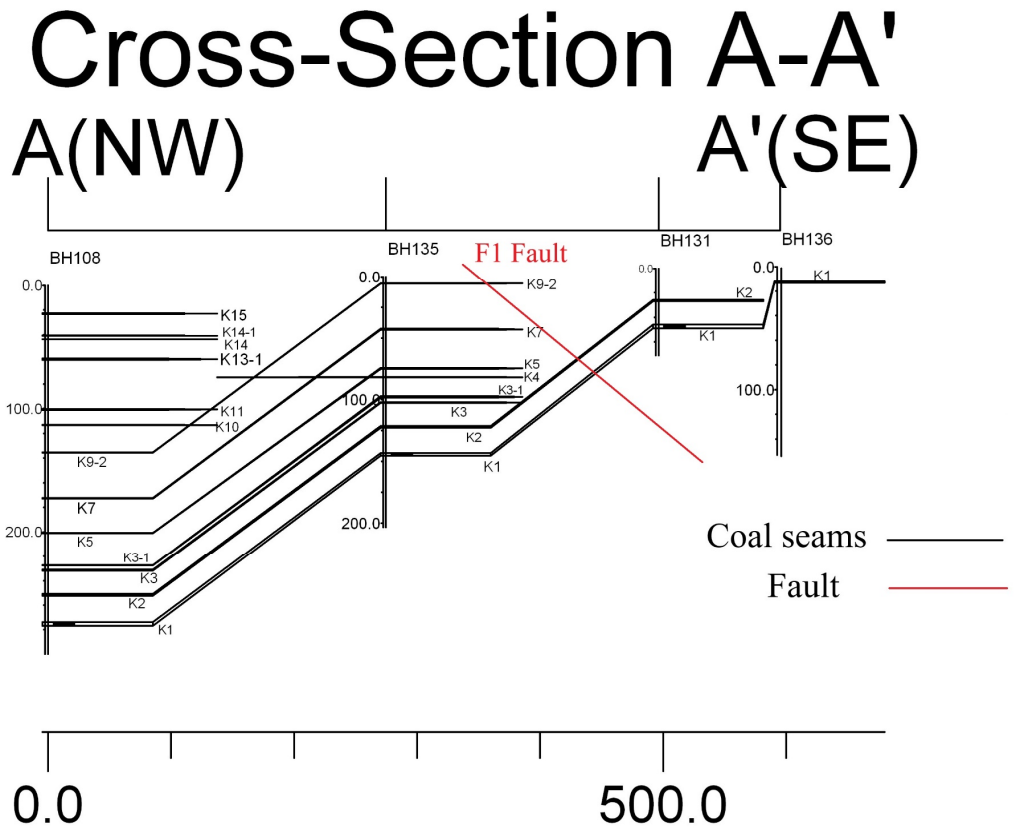

Figure 5. Section A-A' in the northwest to southeast direction between boreholes 108, 135, 131 and 136

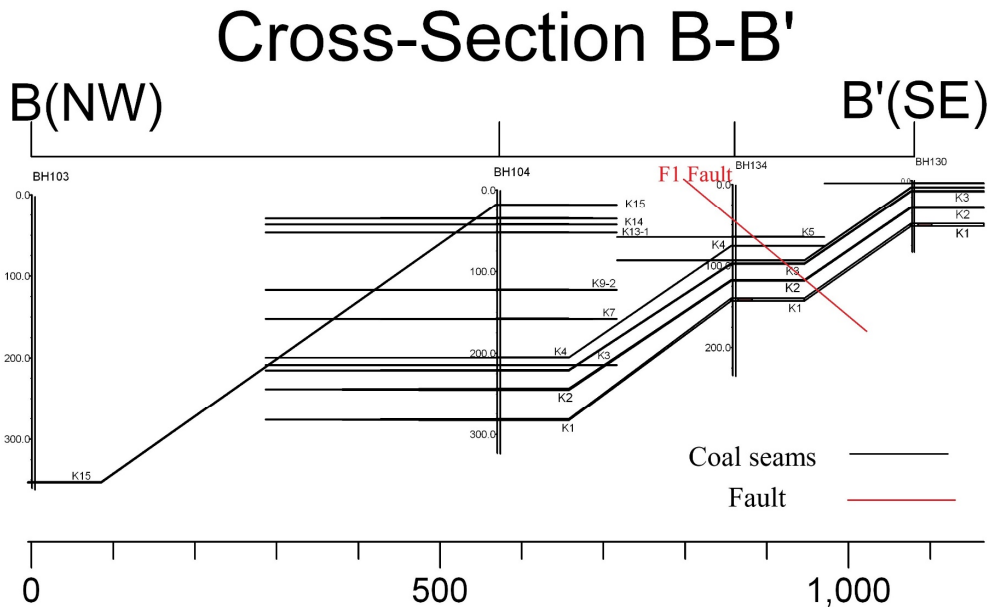

Figure 6. Section B-B' in the northwest to southeast direction between boreholes 103, 104, 134 and 130.

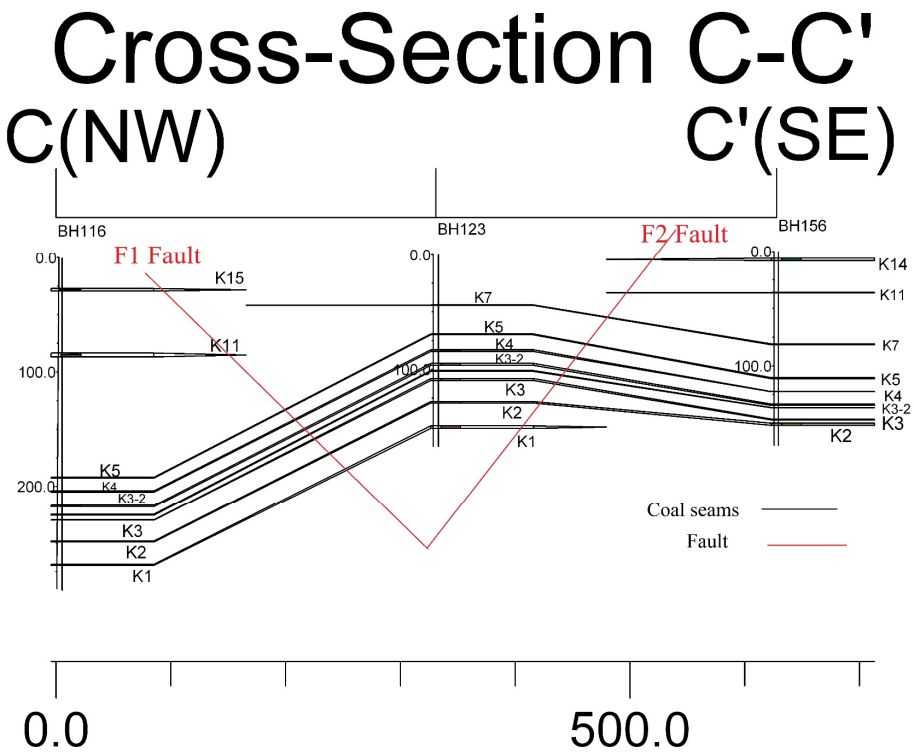

Figure 7. Section C-C' in the northwest to southeast direction between boreholes 116, 123 and 156.

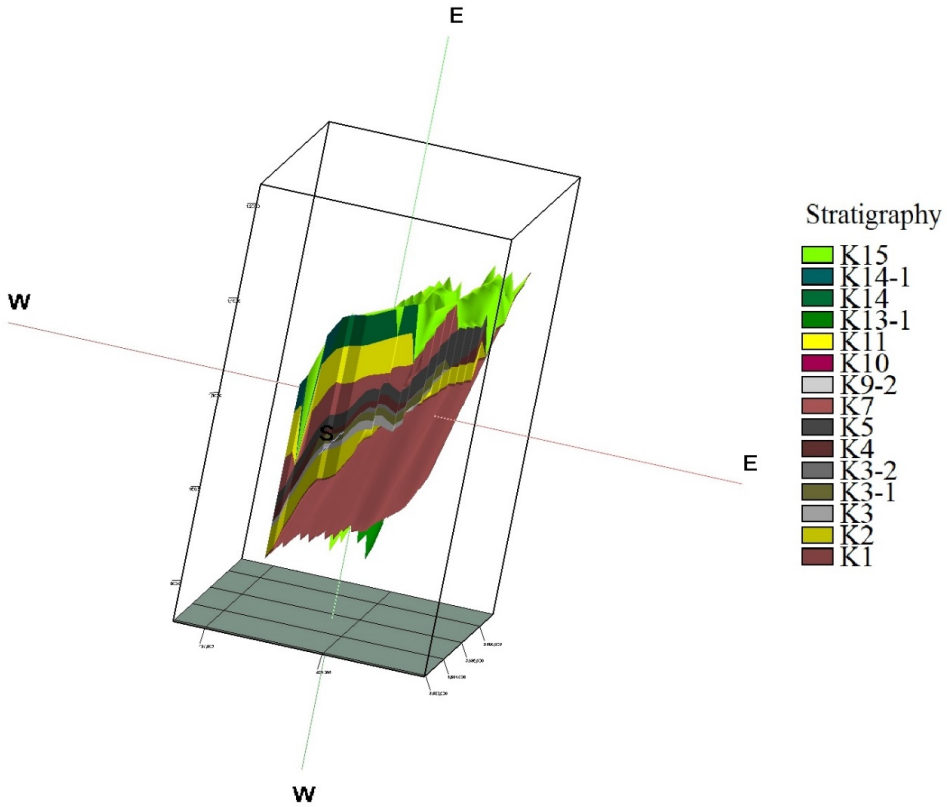

Figure 8. 3D model of target seams that shows pop up structure in North Kochakali coal deposit

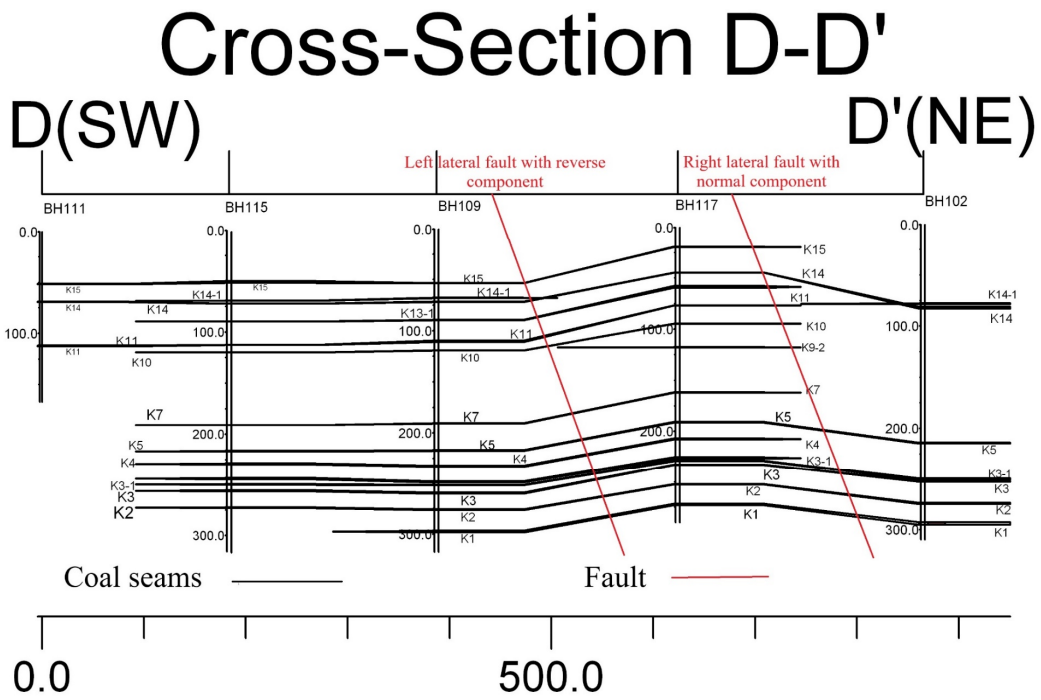

Figure 9. Section D-D' in the southeast to northwest direction between boreholes 111, 115, 109, 117 and 102.

3. Data and methods

In this research, 28 samples (K1S1, K1K2, K1S3, K1S4, K1S5, K2, K2S1, K2S3, K2S4, K5S1, K5-3S1, K5-3S2, K5-3S3, K5-3S4, K5-3S5, K7S2, K7S3, K7S4, K7S5, K32S2, K32S3, K32S4, K32S5, K33S1, K34S1, K34S2, K34S3, and K35S1) were taken from the extraction pits (Figure 10). There are four mining pits in North Kochakali coal deposit, where the mining operations are being carried out in the open pit, and it was tried to take samples from all the outcrops of the coal seams in these mining pits (Figure 11). Samples were placed in plastic bags immediately after sampling and were analyzed by inductively coupled plasma mass spectrometry (ICP-MS) to measure the concentrations of lithium and REEs. By using the concentrations of these elements, Concentration-Number (C-N), Concentration-Area (C-A) fractal models, and geochemical anomalies of REEs and lithium were investigated in the mining area of Norh Kochakali coal mine. For this purpose, first, four C-N fractal models (LiC –N, HREEC-N, LREEC-N, and ΣREEC –N) and four C-A fractal models (LiC –A, HREEC-A, LREEC-A, and ΣREEC –A) were created. Then, 2D and 3D models of the sampling area (mining area) were made by Rockwork 17 software based on C-N and C-A fractal graphs. Finally, two fractal models of C-N and C-A were compared with each other in terms of application in the separation of anomalous areas from the background in the North Kochakali coal deposit.

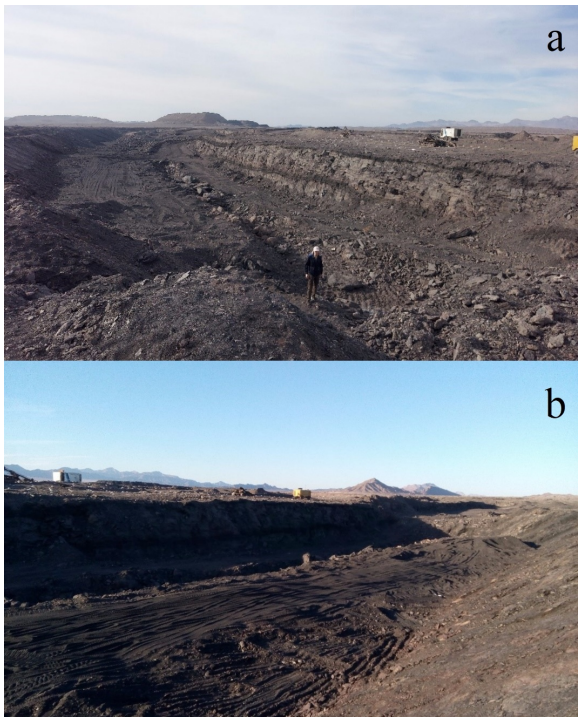

Figure 10. Mining pits of North Kochakali coal deposit, a- K32 seam extraction pit b- K7 seam extraction pit

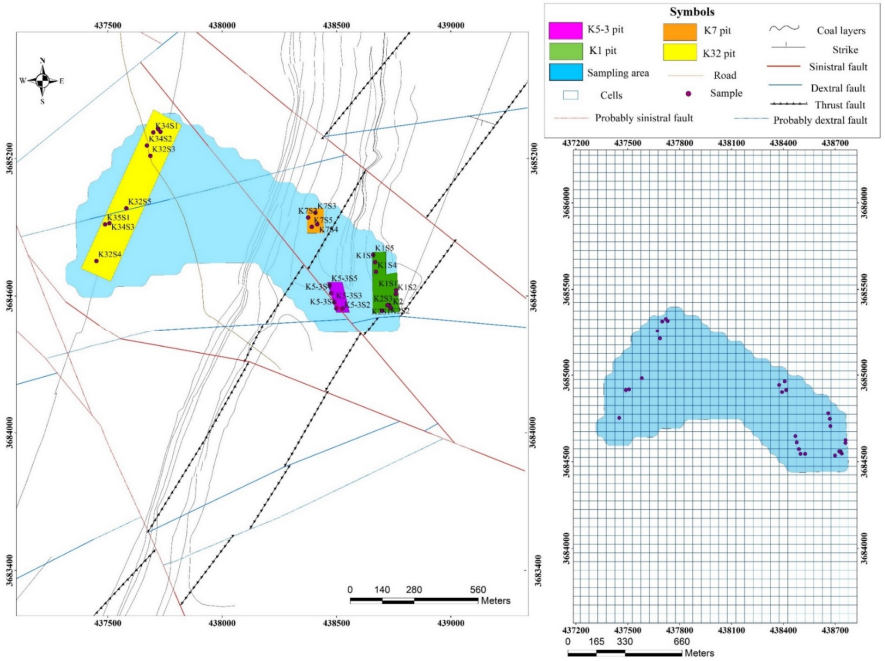

Figure 11. Map of faults, mining pits and mining area in North Kochakali coal deposit.

According to the results of the analysis and calculation of HREEs, LREEs and ΣREEs concentrations in the mining area of North Kochakali coal deposit, the concentrations of LREEs varies from 67.9 ppm to 424.4 ppm, the highest concentration is related to K2 sample and the lowest is related to K5-3S5 sample. In HREEs, K5-3S3 sample has the highest concentration and K5-S1 sample has the lowest concentration. The concentrations of the total amount of rare earth elements (ΣREEs) reached to 627 ppm which corresponds to the K2 sample. Lithium concentrations also vary from 29 ppm to 355 ppm, K5-3S5 sample has the lowest concentrations and the K7S4 sample has the highest concentrations (Table 1).

Table 1. Samples number and concentrations of HREEs, LREEs, ΣREEs and lithium in North kochakali coal deposit

No	Element	HREEs (ppm)	LREEs (ppm)	ΣREEs (ppm)	Li (ppm)
1	K1S1	53.09	205.87	258.96	161
2	K1S2	45.76	274.45	320.21	181
3	K1S3	53.82	209.81	263.63	186
4	K1S4	63.79	234.83	298.62	213
5	K1S5	39.21	193.96	233.17	111
6	K2	202.82	424.4	627.22	277
7	K2S1	61.5	290.67	352.17	234
8	K2S2	63.26	286.77	350.03	237
9	K2S3	45.55	215.64	261.19	99
10	K5-S1	38.42	137.03	175.45	55
11	K5-3S1	53.28	179.88	233.16	143
12	K5-3S2	139.71	355.64	495.35	225
13	K5-3S3	207.97	320.04	528.01	343
14	K5-3S4	132.52	184.6	317.12	175
15	K5-3S5	43.14	67.94	111.08	29
16	K7S2	81.72	322.4	404.12	194
17	K7S3	100.14	230.19	330.33	302
18	K7S4	55.36	166.26	221.62	355
19	K7S5	59.17	228.33	287.5	264
20	K32S2	56.42	272.02	328.44	233
21	K32S3	59.42	286.57	345.99	235
22	K32S4	80.4	121.52	201.92	102
23	K32S5	110.21	280.55	390.76	140
24	K33S1	129	289.06	418.06	192
25	K34S1	47.87	219.88	267.75	221
26	K34S2	92.38	290.21	382.59	264
27	K34S3	74.21	320.22	394.43	172

3.1. Concentration-Number fractal model

Concentration–number (C–N) method was first introduced by [52] and widely used to represent different geochemical populations. general form of this model is as follows:

$$N(\geq\rho) \propto \rho^{-D} \quad (1)$$

N(≥ρ) indicates the sample numbers with Li and REEs concentration greater than or equal to the ρ value. D is the fractal dimension for Li and REEs concentrations, and ρ represent element concentrations. The break points in the logarithmic diagrams (between teach lines segment) and values of ρ indicate the threshold values that are used to separate the anomaly from the background [62].

3.2. Concentration-Area fractal model

Concentration-Area fractal model was first proposed by [50]. This model is a very suitable technique for modeling geochemical anomalies and has many applications in separating anomalies from the background. General form of this model is as follows:

$$A(>\rho) \propto \rho^{-D} \quad (2)$$

A(> ρ) is the cumulative area enclosed by Li and REEs concentrations greater than ρ value, and D indicate fractal dimensions corresponding to different values of ρ. The separation of anomalies into different geochemical groups in this model is done by the threshold values placed between the different line segments in the Concentration-area logarithmic graph [63, 53]. To calculate A, the sampling area is divided into cells with the same dimensions (Figure 11). These cells have the same area, so they were used as the area containing the specific concentrations (Li, HREEs, LREEs, ΣREEs)

4. Results and discussion

by using Li concentrations and cumulative number of samples LiC-N log-log fractal graph was drawn (Figure 12). Base on C-N log-log fractal diagram, 4 different geochemical groups (Low, Moderate, High and very high) were calculated (Table 2).

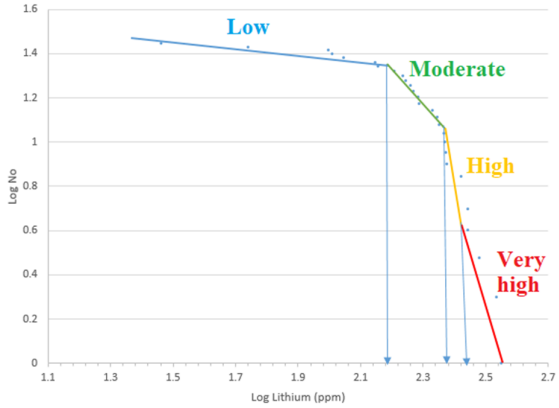

Figure 12. LiC-N fractal graph

Table 2. Different geochemical group base on LiC –N graph

Category	Low	Moderate	High	Very high
Lithium (ppm)	151.3>	151.3-240	240-269	**269<**

Fractal model based on LiC-N log-log fractal graph in sampling area shows than low concentration group (151.3ppm>) just existed in southwest and southeast of sampling area. Very high geochemical group (269ppm<) is just located in east part of sampling area and is surrounded by high geochemical group (240.269ppm). Most parts of the sampling area have a moderate concentration range (151.3-240ppm) (Figure 13).

The amounts of LREEs, HREEs, and the total amount of rare earth elements (ΣREEs) were calculated based on each concentration of REEs. Then three C-N log-log fractal graphs (HREEC –N, LREEC –N, and ΣREEC –N) were drawn for these elements (Figs 14, 15, and 16). C-N log-log fractal graphs show that 4 different geochemical groups were obtained for LREEs, HREEs, and ΣREEs (Tables 3, 4, and 5).

Table 3. Different geochemical group base on HREEC –N graph

Category	Low	Moderate	High	Very high
HREEs (ppm)	52>	52-66	66-138	**138<**

Table 4. Different geochemical group base on LREEC –N graph

Category	Low	Moderate	High	Very high
LREEs (ppm)	182>	182-275	275-302	**302<**

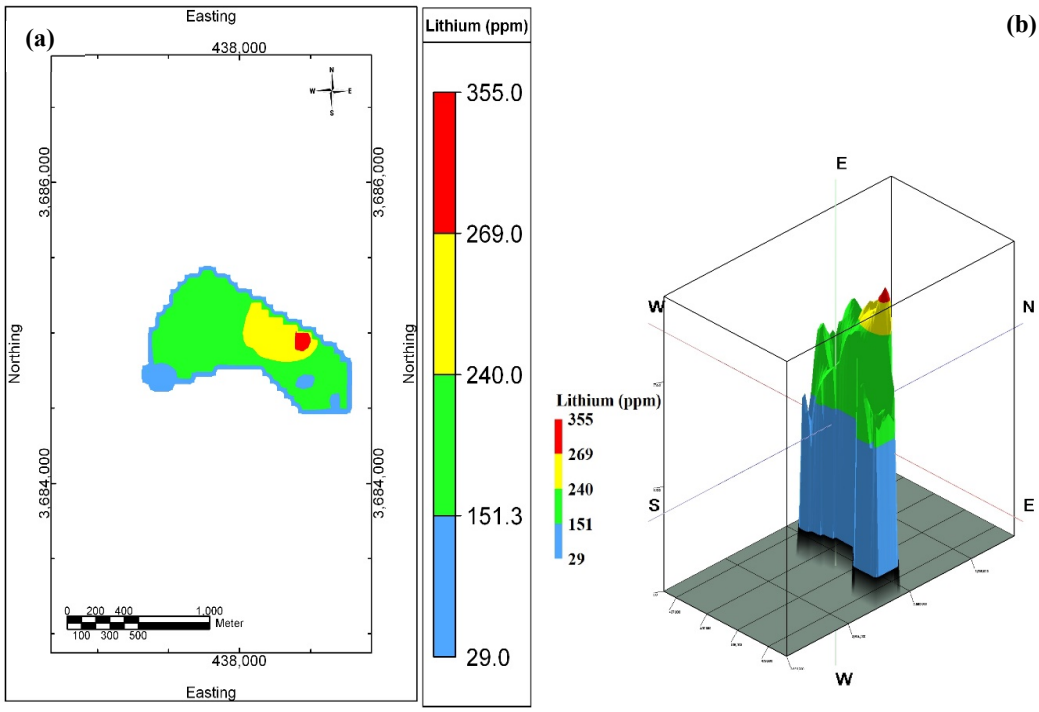

Figure 13. Modeling of sampling area based on LiC –N fractal graph a-2D model b-3D model

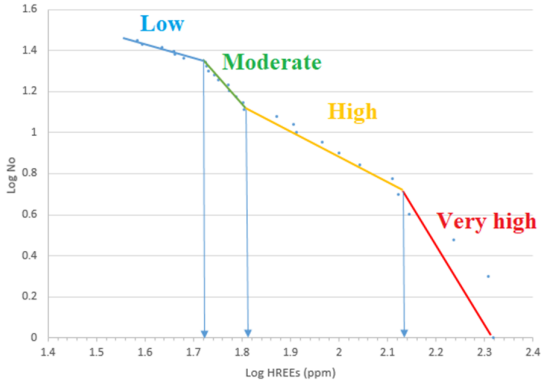

Figure 14. HREEC-N fractal graph

2D and 3D modeling of sampling area base on HREEC –N fractal model show that high geochemical group is located in most parts of the sampling area. In other words, most parts of the mining areas have a concentration between 66-138 ppm. The low geochemical group (52 ppm>) is located only in the eastern part of the sampling area and is surrounded by the moderate geochemical group (52-66ppm) (Figure 17).

LREEC –N fractal model in sampling area shows that high (275-302ppm) and very high (302ppm>) geochemical groups are located in the western part of the sampling area, and most parts of the sampling area are surrounded by the moderate geochemical group (182-275ppm). Low geochemical group (182ppm>) is located only in small parts of the southwest and southeast of the area (Figure 18).

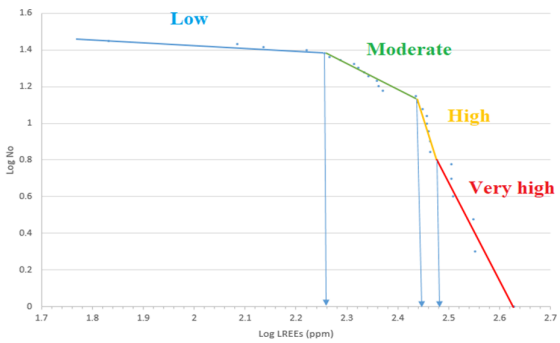

Figure 15. LREEC-N fractal graph

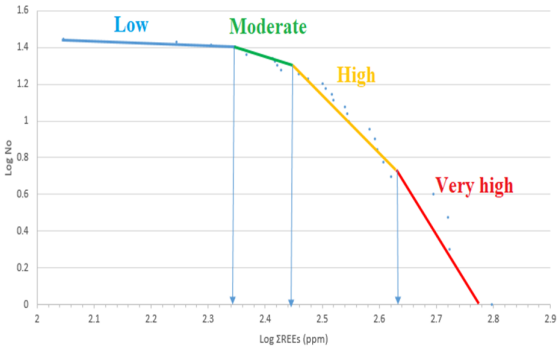

Figure 16- ΣREEC-N fractal graph

Table 5. Different geochemical group base on ΣREEC –N graph

Category	Low	Moderate	High	Very high
ΣREEs (ppm)	219>	219-275	275-436	**436<**

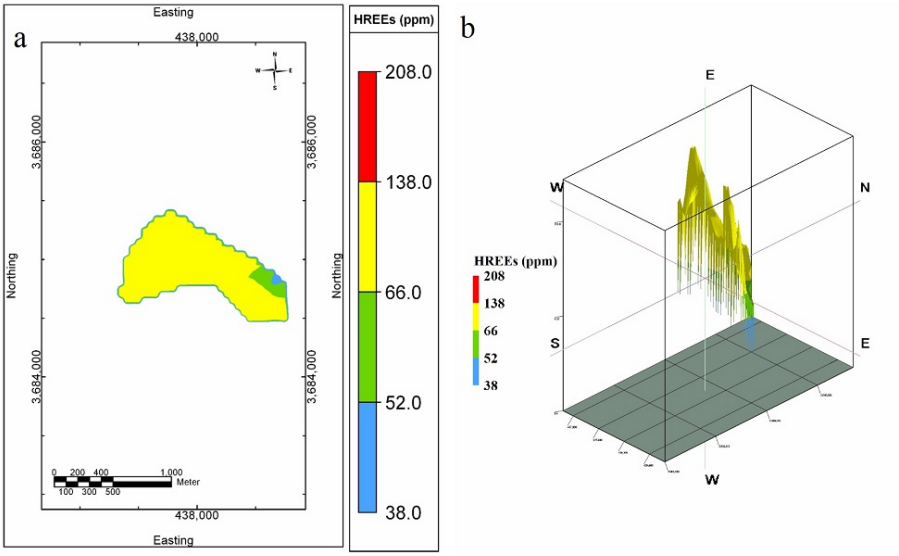

Figure 17. Modeling of sampling area based on HREEC –N fractal graph a-2D model b-3D model

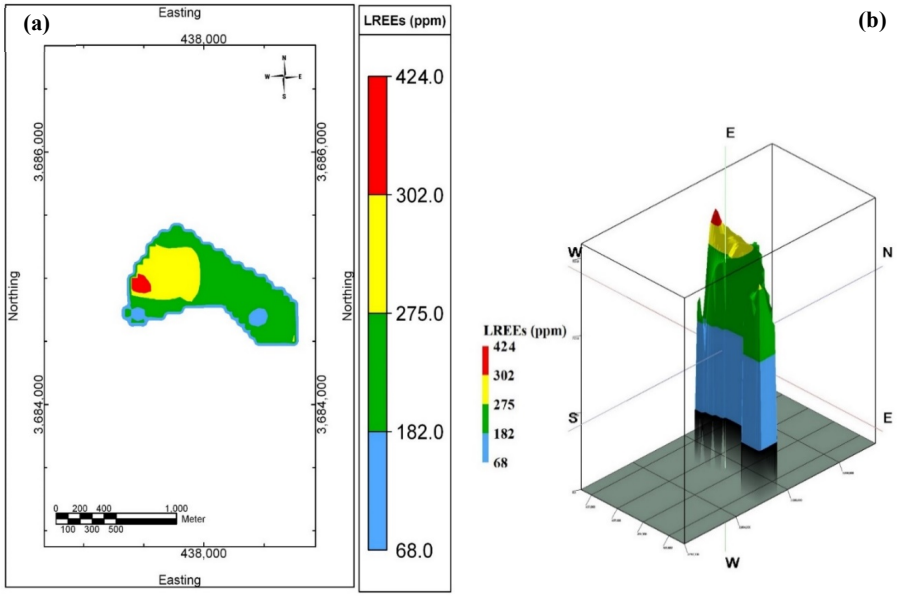

Figure 18. Modeling of sampling area based on LREEC –N fractal graph a-2D model b-3D model

In 3D and 2D modeling of sampling area based on ΣREEC –N fractal model, very high geochemical group (436 ppm<) is very limited and is located only in a small area in the western part of the sampling area. The high geochemical group (275 ppm-436 ppm) is present in most parts of the sampling area and moderate geochemical group (219 ppm- 275 ppm) is located only in a small part of the east and southwest of the sampling area (Figure 19).

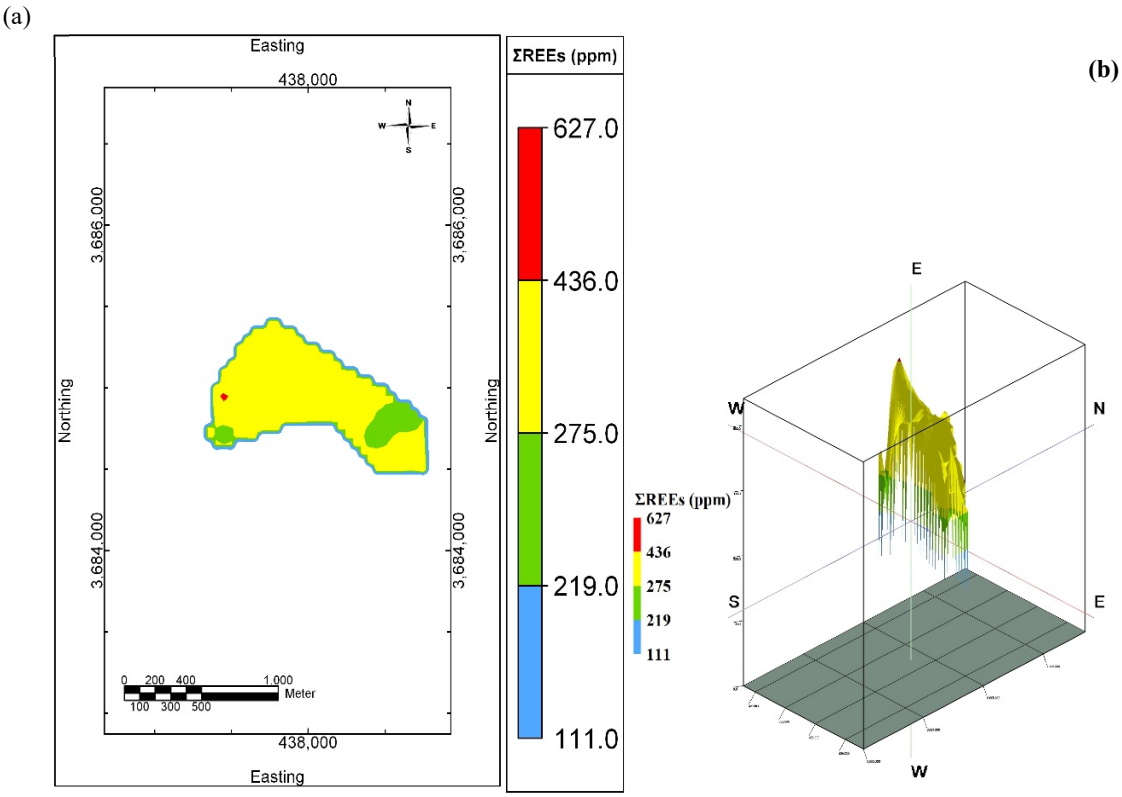

Figure 19. Modeling of sampling area based on ΣREEC –N fractal graph a-2D model b-3D model

The Concentration-Area logarithmic graph (LiC –A fractal graph) for the lithium element was drawn by the concentrations of lithium and the area containing these concentrations (Figure 20). LiC –A fractal graph shows 4-line segments and 3 threshold values that show different geochemical groups, so 4 different geochemical groups (low, moderate, high and very high) were obtained for lithium element (Table 6).

By using LiC –A fractal graph, 2D and 3D models of sampling area (mining area of North Kochakali coal deposit) were prepared. This model shows that concentrations lower than 166 ppm and 219 ppm, which are identified as low and moderate geochemical groups, are accumulated in the southeast and southwest parts of the sampling area but the high concentrations of lithium are accumulated in the northern part and this part has the highest concentrations of lithium. Concentrations more than 251 ppm (very high geochemical group) which were obtained as the highest concentrations level based on LiC –A fractal graph, are located in the northeast of the sampling area (Figure 21).

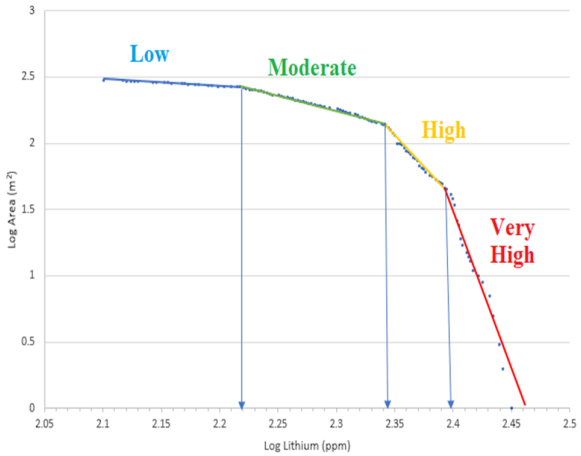

Figure 20. LiC –A fractal graph

Table 6. Different geochemical group base on LiC –A graph

Category	Low	Moderate	High	Very high
Lithium (ppm)	166>	166-219	219-251	**251<**

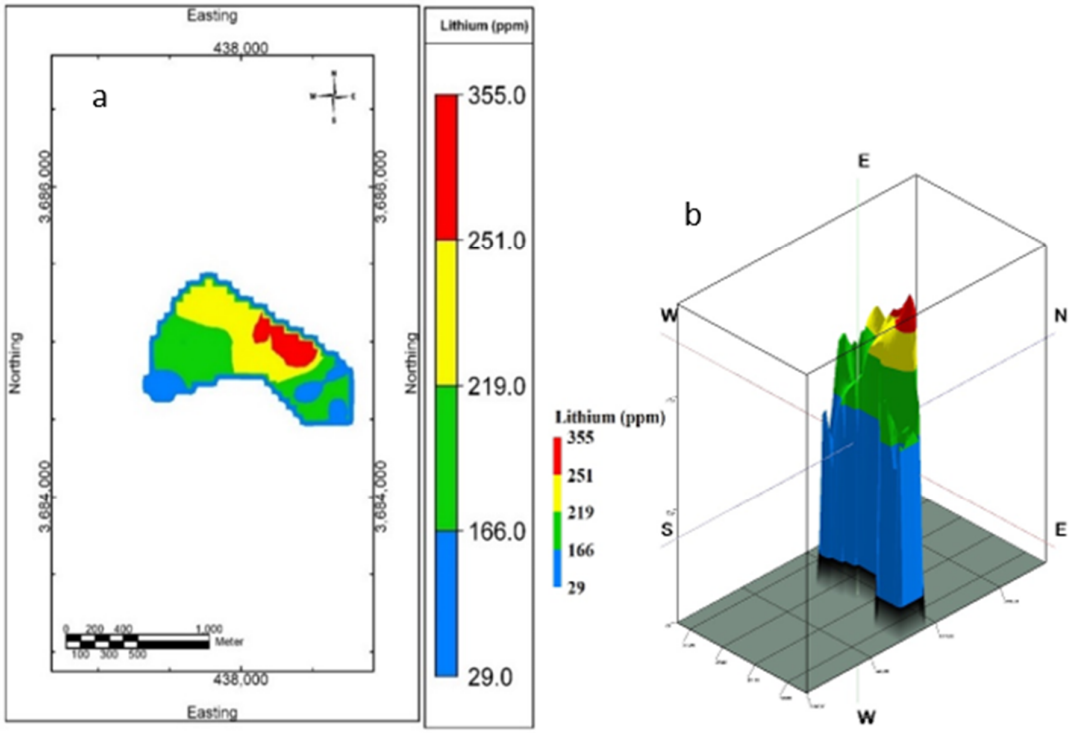

Figure 21. Modeling of sampling area based on LiC –A fractal graph a-2D model b-3D model

Three fractal graphs including: HREEC –A for heavy rare earth elements (HREEs), LREEC –A fractal graph for light rare earth elements (LREEs) and ΣREEC –A fractal graph for total amounts of rare earth elements (ΣREEs) were drawn based on the concentrations of HREEs, LREEs and ΣREEs and the area containing these concentrations (Figs 22, 23, and 24).

All three C-A fractal graphs show 4 different geochemical groups, and based on this, the concentrations frequency of each of the rare earth elements (HREEs, LREEs and ΣREEs) were divided into four geochemical groups including: low, medium, high and very high (Tables 7, 8, and 9).

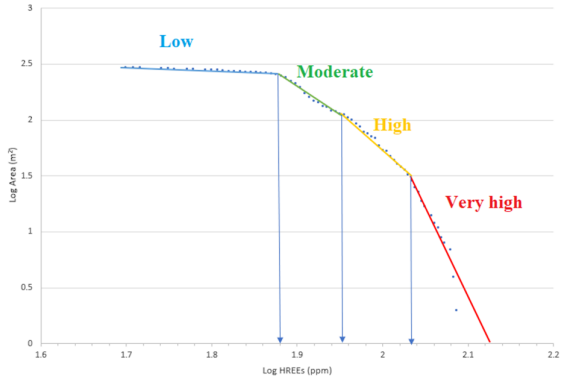

Figure 22. HREEC –A fractal graph

Table 7. Different geochemical group base on HREEC –A graph

Category	Low	Moderate	High	Very high
HREEs (ppm)	76>	76-89	89-110	**110<**

Table 8. Different geochemical group base on LREEC –A graph

Category	Low	Moderate	High	Very high
LREEs (ppm)	200>	200-240	240-275	**275<**

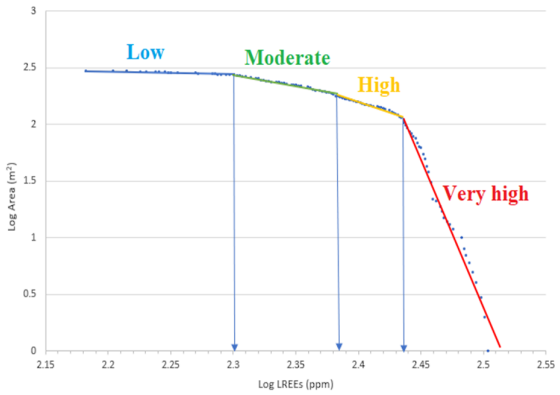

Figure 23. LREEC –A fractal graph

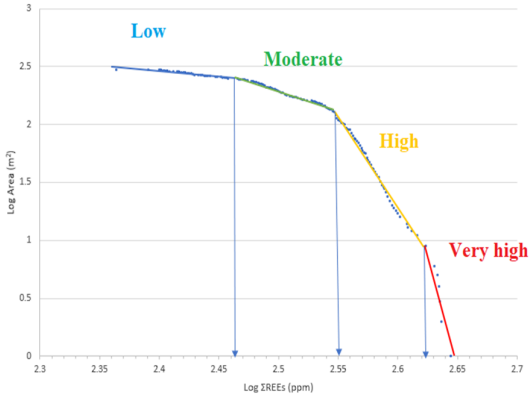

Figure 24. ΣREEC –A fractal graph

Table 9. Different geochemical group base on ΣREEC –A graph

Category	Low	Moderate	High	Very high
ΣREEs (ppm)	288>	288-355	355-426	**426<**

The 2D and 3D models of the distribution of HREEs based on the C-A fractal graph (HREEC –A fractal graph) indicate that the northern parts of the sampling area have the lowest amount of concentrations and the low and moderate geochemical groups are located in this part. The high and very high geochemical groups that have the highest amounts of HREEs are concentrated in the southeastern and western parts of sampling area (Figure 25).

The 2D and 3D models were created for LREEs and ΣREEs based on C-A fractal graphs (LREEC –A and ΣREEC –A). These two models are very similar to each other and in both high and very high concentrations (high and very high geochemical groups) are located in the west and a small part of the southeast of the sampling area and the other parts are surrounded by the lower and middle geochemical groups (Figs 26 and 27).

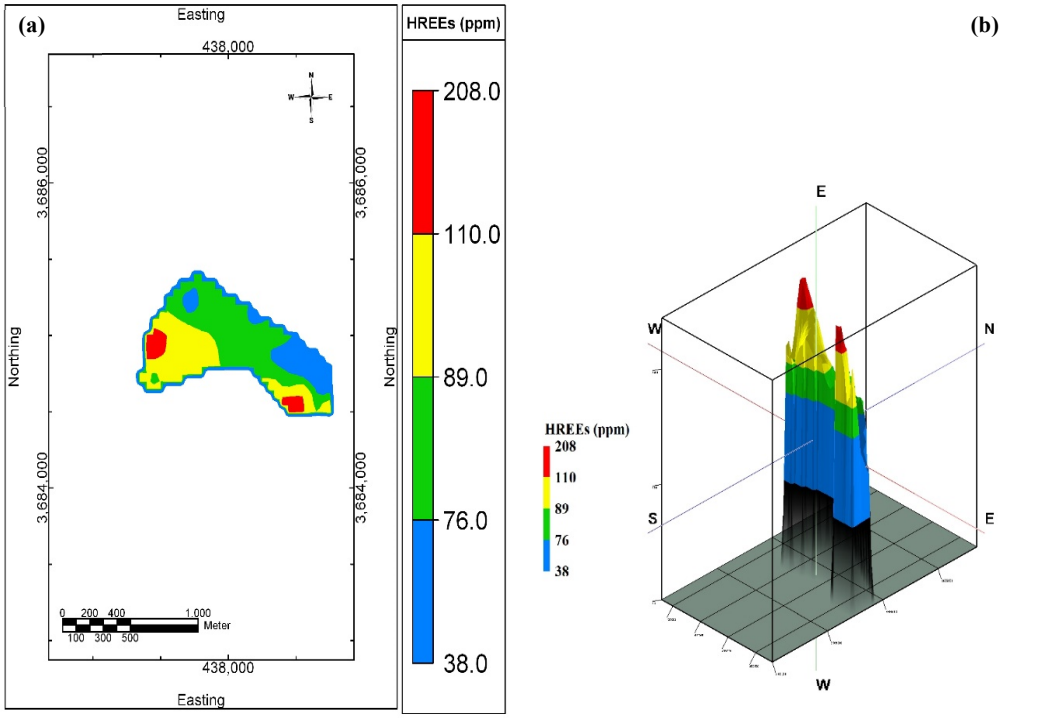

Figure 25. Modeling of sampling area based on HREEC –A fractal graph a-2D model b-3D model

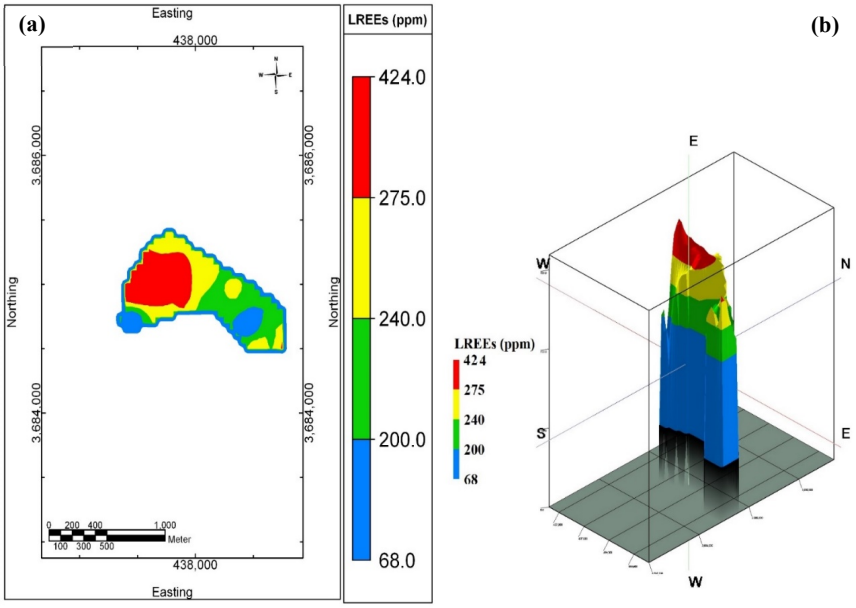

Figure 26. Modeling of sampling area based on LREEC –A fractal graph a-2D model b-3D model

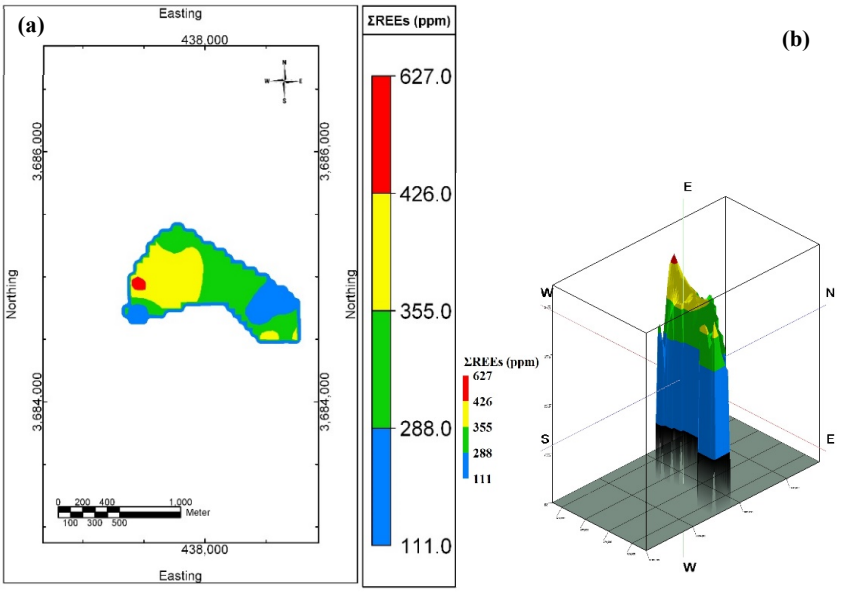

Figure 27. Modeling of sampling area based on ΣREEC –A fractal graph a-2D model b-3D model

The comparison of the threshold values obtained from the C-A and C-N fractal models shows that in the C-A fractal model, the third threshold values that indicate the very high and high geochemical groups and generally anomalous for REEs and lithium in the mining area of North Kochakali are lower than C-N fractal model. Also, first threshold values in the C-N fractal model are lower than the C-A fractal model of the area (Table 10).

Table 10. Comparison table of threshold values in C-N and C-A fractal models.

C-N fractal model			C-A fractal model			Elements
First threshold value	Second threshold value	Third threshold value	First threshold value	Second threshold value	Third threshold value	
151	240	269	166	219	251	Lithium
52	66	138	76	89	110	HREEs
182	275	302	200	240	275	LREEs
219	275	436	288	355	426	ΣREEs

Many researchers have separated anomalies from the background by using fractal models [26, 64-69] but the separation of lithium and REEs anomalies in coal by using C-A and C-N fractal models have been done for the first time.

[70], after investigating the main sources of lithium in Chinese coal mines, concluded that aluminum silicates and clays are among the main lithium-bearing minerals in coal, and geological factors such as tectonics and geological history of the coal basin, stable weathering, steady movement of surface water, and constant supply of lithium and aluminum are the main factors of lithium enrichment in coal. [71] have considered the enrichment of clay-type lithium in Central Inner Mongolia as a result of absorption in the form of interlayer ions along with altered materials such as montmorillonite and chlorite. In general, phosphates, and carbonates are among the most important minerals containing REEs and REY in coal [72-74]. [74] showed that geological factors and different deposition pathways are the most important factors in the distribution and chemistry of REEs in coal. [75] have considered multi-stage hydrothermal processes as the cause of the enrichment of REEs in northeastern Sichuan Basin, China. Therefore, geological factors such as tectonics and geological history of the study area play a significate role in the enrichment of lithium and REEs in coal.

The average concentration of lithium element in the coal seams of North Kochakali is 200.7 ppm, while the average statistical value of this element is 31.8 ppm [76]. Also, the average concentration of lithium in the Bije coal basin in China is about 87 ppm [77]. So, the high concentration of lithium in North Kochakali coal mine indicates the high enrichment of this element in North Kochakali coal deposit.

REEs were branched into critical (Y, Tb, Dy, Er, Eu and Nd), uncritical (Pr, Sm, Gd and La) and excessive (Lu, Yb, Tm and Ce) [11]. There is an index called outlook coefficient in coal (C_{Out1}). This index shows the economical level of REEs in coal and is calculated as follows:

$$C_{Out1} = (\text{Critical REEs}/\ \Sigma\text{REEs})/(\text{Excessive REEs}/\ \Sigma\text{REEs}) \quad (1)$$

If the C_{Out1} index has values lower than 0.7, it is non-economic coal; if it has values between 0.7 and 2.4, it is semi-economic coal; and if it has values higher than 2.4, it is economic coal [6]. The average concentration of ΣREEs in North Kochakali coal mine is 333 ppm, the average concentrations of critical and excessive REEs in this mine are 128 ppm and 88 ppm, respectively. So, the C_{Out1} index for REEs in North Kochakali coal mine is equal to 1.45, which is semi-economic coal.

The average concentration of ΣREEs in North Kochakali coal mine is almost 120 ppm more than the average concentration of these elements in Parvadeh coal mine and 90.8 ppm more than the average concentration of REEΣs in the continental crust. The average values of HREEs in North Kochakali (Except for the value of the Ho element which has a low concentration in North Kochakali mine) are very close to the global average values of REEs in world coal ash (Table. 11).

Table 11. Comparison table of the average values of ΣREEs in North Kochakali Coal mine with continental crust [78], world coal ash [79] and Parvadeh coal mine [80].

Elements	Y	Gd	Tb	Dy	Ho	Er	Tm	Yb	Lu	Sc	La	Ce	Pr	Nd	Sm	Eu	REEΣ
North Kochakali Coal mine	41.6	13.4	3.2	12.3	0.9	6.3	0.9	4	0.8	36.5	39	82	14	59.9	13.5	3.2	333
Central Iran (Parvadeh Coal Mine)	20.34	6.75	1.16	5.25	1.26	2.82	0.1	3.24	0.12	17.82	33.26	68.48	-	19.22	31	1.96	212.7
continental crust	33	6.2	1.2	5.2	1.3	3.5	5.52	3.2	0.8	22	39	66.5	9.2	41.5	7.05	2	242.17
World coal ash	57	16	2.1	15	4.8	6.4	2.2	6.9	1.3	24	76	140	26	75	14	2.6	469.3

5. Conclusions

Comparison of 2D and 3D models and logarithmic graph in two C-A and C-N models shows that in the C-A fractal model, the third threshold values indicate a very high and high geochemical groups are lower, and in this model, geochemical groups and anomalies are better separated.

C-A and C-N fractal models show that the western and southeast parts of mining area in North Kochakali have the highest concentrations of HREEs, LREEs and ΣREEs. Therefore, these parts are considered as anomalies parts for REEs due to

having the highest concentrations of these elements. These parts are close to the right-lateral faults with a normal component. Since the faults in the North Kochakali were formed after the formation of coal seams (according to the displacement of the target seams by the faults), it can be concluded that the mineralization of REEs in the North Kochakali coal deposit is epigenetic.

Based on the C-A and C-N fractal models, the northeastern part of the mining area in North Kochakali is considered as an anomalous part of this element due to having the highest concentration of lithium element. Considering that the Hojedk Formation was formed in a back-arc basin related to subduction of Neotethys ocean and the presence of normal faults at the bottom of the basin, which causes upward movement of fluids and igneous materials containing lithium and other elements, the enrichment of lithium North Kochakali area is related to the tectonic history of Hojedk Formation and the faults in the North Kochakali area have only caused the displacement of this element and its enrichment in the northeastern part.

Western and southeastern parts of mining area in North Kochakali have the highest enrichment of HREEs, LREEs and ΣREEs and the northeast part has the highest enrichment of lithium element. Due to their higher economic value of these parts, western, southeastern and northeast parts of mining area in North Kochakali coal deposit should be considered more in mining operations and waste depots.

Acknowledgment

The authors would like to thank Dr. Zahra Aghaei from Falat Zarin Kimia company for authorizing the access to the North Kochakali data of drilled boreholes.

Refferences

[1]. Hustrulid, W., Kuchta, M., & Martin, R. (2006). Open Pit Mine Planning and Design. *CRC Press Taylor & Francis Group*, New York, 1308.

[2]. Yasrebi, A.B., Wetherelt, A., Foster, P., & Afzal, P. (2011). Determination and Analysis of final pit limit of Esfordi phosphate open pit mine. *22nd World Mining Congress & Expolration, Istanbul, Turkey*, *22*, 513-522.

[3]. Yasrebi, A.B., Hezarkhani, A., & Afzal, P. (2017). Application of Present Value-Volume (PV-V) and NPV-Cumulative Total Ore (NPV-CTO) fractal modelling for mining strategy selection. *Resources Policy*, *53*(3), 384-393.

[4]. Montross, S.N., Yang, J., Britton, J., McKoy, M., & Verba. C. (2021). Leaching of Rare Earth Elements from Central Appalachian Coal Seam Underclays. *Minerals*, *10*(6), 577.

[5]. Huang, S., Ning, S., Zhang, D., Cai, Y., Yan, X., Liu, K., & Xiaotao, X. (2023). Rare Earth Element Characteristics in Coal Ash from the Jungar Energy Gangue Power Plant, Inner Mongolia, China. *Minerals*, *13*(9), 1212.

[6]. Dai, S., Xie, P., Jia, S., Ward, C.R., Hower, J.C., Yan, X., & French, D. (2017). Enrichment of U-Re-V-Cr-Se and rare earth elements in the Late Permian coals of the Moxinpo Coalfield, Chongqing, China: Genetic implications from geochemical and mineralogical data. *Ore Geology Reviews*, *80*, 1–17.

[7]. Zhao, C., Liu, B., Xiao, L., Li, Y., Liu, S., Li, Z., Zhao, B., Ma, J., Chu, G., Gao, P., & Sun, Y. (2017). Significant enrichment of Ga, Rb, Cs, REEs and Y in the Jurassic No. 6 coal in the IQE Coalfield, northern Qaidam Basin, China—A hidden gem. *Ore Geology Reviews*, *83*, 1–13.

[8]. Dai, S., & Finkelman, R.B. (2018). Coal as a promising source of critical elements: Progress and future prospects. *International Journal of Coal Geology*, *186*, 155–164.

[9]. Zhao, L., Dai, S., Nechaev, V.P., Nechaeva, E.V., Graham, I.T., French, D., & Sun, J. (2019). Enrichment of critical elements (Nb-Ta-Zr-Hf-REE) within coal and host rocks from the Datanhao mine, Daqingshan Coalfield, northern China. *Ore Geology Reviews*, *111*, 102951.

[10]. Seredin, V.V., & Finkelman, R.B. (2008). Metalliferous coals: a review of the main genetic and geochemical types. *International Journal of Coal Geology*. *76*(4), 253–289.

[11]. Seredin, V.V., & Dai, S. (2012). Coal deposits as potential alternative sources for lanthanides and yttrium. *International Journal of Coal Geology*, *94*, 67–93.

[12]. Eskenazy, G.M. (1987). Rare earth elements in a sampled coal from the Pirin deposit, Bulgaria. *International Journal of Coal Geology*, *7*(3), 301–314.

[13]. Wang, W., Qin, Y., Sang, S., Zhu, Y., Wang, C., & Weiss, D.J. (2008). Geochemistry of rare earth elements in a marine influenced coal and its organic solvent extracts from the Antaibao mining district, Shanxi, China. *International Journal of Coal Geology*, *76*(3), 309–317.

[14]. Pazand, K. (2015). Rare earth element geochemistry of coals from the Mazino Coal Mine, Tabas Coalfield, Iran. *Arabian Journal of Geosciences*, *8*(12), 10859–10869.

[15]. Dai, S., Li, D., Chou, C.L., Zhao, L., Zhang, Y., Ren, D., Ma, Y., & Sun, Y. (2008). Mineralogy and geochemistry of boehmiterich coals: new insights from the Haerwusu Surface Mine, Jungar Coalfield, Inner Mongolia, China. *International Journal of Coal Geology*, *74*(3-4), 185-202.

[16]. Dai, S., Zou, J., Jiang, Y., Ward, C.R., Wang, X., Li, T., Xue, W., Liu, S., Tian, H., Sun, X., & Zhou D. (2012). Mineralogical and geochemical compositions of the Pennsylvanian coal in the Adaohai Mine, Daqingshan Coalfield, Inner Mongolia, China: Modes of occurrence

and origin of diaspore, gorceixite, and ammonian illite. *International Journal of Coal Geology*, *94*, 250-270.

[17]. He, H.T., Wang, J.X., Xing, L.C., Zhao, S.S., He, M.Y., Zhao, C.L., & Sun, Y.Z. (2020). Enrichment mechanisms of lithium in the No. 6 coal seam from the Guanbanwusu Mine, Inner Mongolia, China: Explanations based on Li isotope values and density functional theory calculations. *Journal of Geochemical Exploration*, *213*, 106510.

[18]. Zhou, M. X., Zhao, L., Wang, X. B., Victor, P., Wang, X. B., Nechaev, V.P., French, D., Spiro, B.F., Graham, I.T., Hower, J.C., & Dai, S.F. (2021). Mineralogy and geochemistry of the Late Triassic coal from the Caotang mine, northeastern Sichuan Basin, China, with emphasis on the enrichment of the critical element lithium. *Ore Geology Reviews*, *139*(11), 104582.

[19]. Watari, T., Nansai, K., & Nakajima, K. (2020). Lithium: Review of critical metal dynamics to 2050 for 48 elements. *Resources, Conservation and Recycling*, *155*, 104669.

[20]. Dai, S.F., Ren, D.Y., Zhang, J.Y., & Hou, X.Q. (2003). Concentrations and origins of platinum 495 group elements in Late Paleozoic coals of China. *International Journal of Coal Geology*, *55*(1), 59–70.

[21]. Dai, S.F., Sun, Y.Z., & Zeng, R.S. (2006). Enrichment of arsenic, antimony, mercury, and 500 thallium in a Late Permian anthracite from Xingren, Guizhou, Southwest China. *International Journal of Coal Geology*, *66*(3), 217–226.

[22]. Munk, L.A., Hynek, S.A., Bradley, D.C., Boutt, D., Labay, K., & Jochens, H. (2016). Lithium Brines: A Global Perspective. In: Rare Earth and Critical Elements in Ore Deposits**.** *Society of Economic Geologists, 18.* 339-365.

[23]. Rossi, C., Bateson, L., Bayaraa, M., Butcher, A., Ford, J., & Hughes, A. (2022). Framework for Remote Sensing and Modelling of Lithium-Brine Deposit Formation. *Remote Sensing*, *14*(6), 1383.

[24]. Daya, A.A. (2012). Reserve estimation of central part of Choghart north anomaly iron ore deposit through ordinary kriging method. *International Journal of Mining Science and Technology*, *22*, 573–577.

[25]. Hashemi, M., & Afzal, P. (2013). Identification of geochemical anomalies by using of number–size (N–S) fractal model in Bardaskan area, NE Iran. *Arabian Journal of Geosciences*, *6*(12), 4785–4794.

[26]. Momeni, S., Shahrokhia, S.V., Afzal, P., Sadeghi, B., Farhadinejada, T., & Nikzade, M.Z. (2016). Delineation of the Cr mineralization based on the stream sediment datautilizing fractal modeling and factor analysis in the Khoy 1:100,000 sheet, NW Iran. *Bulletin Of The Mineral Research and Exploration*, *152*, 143-151.

[27]. Afzal, P., Ahmadi, K., & Rahbar, K. (2017). Application of fractal-wavelet analysis for separation of geochemical anomalies. *Journal of African Earth Sciences*, *128*, 27–36.

[28]. Alipour Shahsavari, M., Afzal, P., & Hekmatnejad, A. (2019). Identification of Geochemical Anomalies Using Fractal and LOLIMOT Neuro-Fuzzy modeling in Mial Area, Central Iran. *Journal of Mining and Environment (JME)*, *11*, 99-117.

[29]. Mandelbrot, B.B. (1982). The fractal geometry of nature. *San Francisco*, CA, 598.

[30]. Sadeghi, B. (2024). Fractals and Multifractals in the Geosciences. *Elsivier*, 302.

[31]. Carranza, E.J.M., Zuo, R., & Cheng, Q. (2012). Fractal/multifractal modelling of geochemicalexploration data. *Journal of Geochemical Exploration*, *122*, 1-3.

[32]. Afzal, P., Alhoseini, S.H., Tokhmechi, B., Kaveh Ahangaran, D., Yasrebi, A.B., Madani, N., & Wetherelt, A. (2014). Outlining of high quality coking coal by concentration–volume fractal model and turning bands simulation in East-Parvadeh coal deposit, Central Iran. *International Journal of Coal Geology*, *127*(1), 88–99.

[33]. Daya, A.K. (2014). Comparative study of C–A, C–P, and N–S fractal methods for separating geochemical anomalies from background: A case study of Kamoshgaran region, northwest of Iran. *Journal of Geochemical Exploration*, *150*, 52–63.

[34]. Zuo, R., & Wang, J. (2016). Fractal/multifractal modeling of geochemical data: a review. *Journal of Geochemical Exploration*, *164*, 33-41.

[35]. Seyedrahimi Niaraq, M., & Hekmatnejad, A. (2020). The efficiency and accuracy of probability graph, spatial statistic and fractal methods in the identification of shear zone gold mineralization: a case study of the Saqqez gold ore district, NW Iran. *Acta Geochim*, *40*(1).

[36]. Dimri, V.P., & Srivastava, R.P. (2005). Fractal modeling of complex subsurface geological structures. In Fractal Behaviour of the Earth System. *Springer*, Berlin Heidelberg, 205.

[37]. Abedi, M., Torabi, S.A., & Norouzi, G.H. (2013). Application of fuzzy AHP method to integrate geophysical data in a prospect scale, a case study: Seridune copper deposit. *Bollettino di Geofisica Teorica ed Applicata*, *54*(2), 145-164.

[38]. Chen, G., Cheng, Q., Liu, T., & Yang, Y. (2013). Mapping local singularities using magnetic data to investigate the volcanic rocks of the Qikou depression, Dagang oilfield, eastern China. *Nonlinear processes in geophysics*, *20*(4), 501-511.

[39]. Wang, W., Zhao, J., & Cheng, Q. (2013). Application of singularity index mapping technique to gravity/magnetic data analysis in southeastern Yunnan mineral district. China. *Journal of Applied Geophysics*, *92*, 39-49.

[40]. Khalajmasoumi, M., Lotfi, M., Afzal, P., Sadeghi, B., Memar Kochebagh, A., Khakzad, A., & Ziazarifi, A. (2015). Delineation of the radioactive elements based on the radiometric data using concentration–area fractal method in the Saghand area, Central Iran. *Arabian Journal of Geosciences*, *8*(8), 6047–6062.

[41]. Salarian, S., Asghari, O., Abedi, M., & Alilou, S.K. (2019). Geostatistical and multi-fractal modeling of geological and geophysical characteristics in Ghalandar

Skarn-Porphyry Cu Deposit, Iran. *Journal of Mining and Environment (JME)*, *10*(4), 1061- 1081.

[42]. Hodkiewicz, P., Weinberg, R., Gardoll, S., & Groves, D. (2005). Complexity gradients in the YilgarnCraton: fundamental controls on crustal-scale fluid flow and the formation of world-class orogenic-gold deposits. *Australian Journal of Earth Sciences*, *52*(6), 831-841.

[43]. Pérez-López, R., & Paredes, C. (2006). On measuring the fractal anisotropy of 2-D geometrical sets: Application to the spatial distribution of fractures. *Geoderma*, *134*(3-4), 402-414.

[44]. Nabilou, M., Arian, M., Afzal, P., Adib, A., & Kazemi Mehrnia, A. (2018). Determination of relationship between magnetic fault lineaments and alteration zones in Bafq Esfordi region, Central Iran. *Episodes*, *41*(3), 143-159

[45]. Adib, A., Nabilou, M., & Afzal, P. (2021). Relationship between Fe-Cu-REEs mineralization and magnetic basement faults using multifractal modeling in Tarom region, NW Iran. *Episodes*, *45*(3), 223-237.

[46]. Masoumi, M., Honarmand, M., & Salimi, A. (2021). Integration of concentration-area fractal model and relative absorption band depth method for mapping hydrothermal alterations using ASTER data. Remote Sensing Applications. *Society and Environment*, *23*(1), 100519.

[47]. Ivanovici, M. (2023). A Multi-Spectral Fractal Image Model and Its Associated Fractal Dimension Estimator. *Fractal Fract*, *7*(3), 238.

[48]. Sim, B.L., Agterberg, F.P., & Beaudry, C. (1999). Determining the cutoff between background and relative base metal contamination levels using multifractal methods. *Computers and Geosciences*, *25*, 1023–1041.

[49]. Afzal, P., FadakarAlghalandis, Y., Khakzad, A., Moarefvand, P., & Rashidnejad Omran, N. (2011). Delineation of mineralization zones in porphyry Cu deposits by fractal concentration–volume modeling. *Journal of Geochemical Exploration*, *108*(3), 220–232.

[50]. Cheng, Q., Agterberg, F.P., & Ballantyne, S.B. (1994). The separation of geochemical anomalies from background by fractal methods. *Journal of Geochemical Exploration*, *51*(2), 109–130.

[51]. Cheng, Q., Xu, Y., & Grunsky, E. (1999). Integrated spatial and spectral analysis for geochemical anomaly separation. In: Lippard, S.J., Naess, A., Sinding-Larsen, R. (Eds.). *Proc of the Conference of the International Association for Mathematical Geology*, *1*, 87–92.

[52]. Hassanpour, S.H., & Afzal, P. (2013). Application of concentration–number (C–N) multifractal modeling for geochemical anomaly separation in Haftcheshmeh porphyry system, NW Iran. *Arabian Journal of Geosciences*, *6*(3), 957–970.

[53]. Sadeghi, B. (2021). Concentration-Area Plot. In: Daya Sagar, B., Cheng, Q., McKinley, J., & Agterberg, F. (eds) Encyclopedia of Mathematical Geosciences. Encyclopedia of Earth Sciences Series. *Springer, Cham*, 169-175.

[54]. Stampfli, G.M., & Borel, G.D. (2002). A plate tectonic model for the Paleozoic and Mesozoic constrained by dynamic plate boundaries and restored synthetic oceanic isochrones. *Earth and Planetary Science Letters*, *196*(1-2), 17–33.

[55]. Wilmsen, M., Fürsich, F.T., Seyed-Emami, K., Majidifard, M.R., & Taheri, J. (2009). The Cimmerian orogeny in northern Iran: tectono-stratigraphic evidence from the foreland. *Terra Nova*, *21*(3), 211 – 218.

[56]. Esmaeily, D., Bouchez, J.L., & Siqueira, R. (2007). Magnetic fabrics and microstructures of the Jurassic Shah-Kuh granite pluton (Lut Block, Eastern Iran) and geodynamic inference. *Tectonophysics*, *439*(1-4), 149–170.

[57]. Wilmsen, M., Fürsich, F.T., Seyed-Emami, K., & Majidifard, M.R. (2009). An overview of the lithostratigraphy and facies development of the Jurassic System on the Tabas Block, east-central Iran. *Geological Society London Special Publications*, *312*(1), 323-343.

[58]. Seyed-Emami, K., Schairer, G., Fürsich, F.T., Wilmsen, M., & Majidifard, M.R. (2000). First record of ammonites from the Badamu Formation at the Shotori Mountains (Central Iran). *Eclogae Geologiae Helvetiae*, *93*(2), 257–263.

[59]. Fürsich, F.T., Wilmsen, M., Seyed-Emami, K., & Majidifard, M.R. (2009). Lithostratigraphy of the Upper Triassic–Middle Jurassic Shemshak Group of Northern Iran. In South Caspian to Central Iran Basins. *Geological Society of London, Special Publication*, *312*(1), 129–60.

[60]. Salehi, M.A., Wilmsen, M., Zamanian, E., Baniasad, A., & Heubeck, C. (2022). Depositional and thermal history of a continental, coal-bearing Middle Jurassic succession from Iran: Hojedk Formation, northern Tabas Block. *Geological Magazine*, *160*(2), 235-259.

[61]. Wilmsen, M., Fürsich, F., Seyed-Emami, K., Majidifard, M., & Zamani-Pedram, M. (2010). Facies analysis of a large-scale Jurassic shelflagoon: the Kamar-e-Mehdi Formation ofeast-central Iran. *Facies*, *56*(1), 59–87.

[62]. Sadeghi, B., Moarefvand, P., Afzal, P., Yasrebi, A., & Saein, L. (2012). Application of fractalmodels to outline mineralized zones in the Zaghia iron ore deposit, Central Iran. *Journal of Geochemical Exploration*, *122*, 9–19.

[63]. Afzal, P., Khakzad, A., Moarefvand, P., RashidnejadOmran, N., Esfandiari, B., & FadakarAlghalandis, Y. (2010). Geochemical anomaly separation by multifractal modeling in Kahang (GorGor) porphyry system, Central Iran. *Journal of Geochemical Exploration*, *104*(1-2), 34–46.

[64]. Shokouh Saljoughi, B., Hezarkhani, A., & Farahbakhsh, E. (2017). A comparative study of fractal models and U-statistic method to identify geochemical anomalies; case study of Avanj porphyry system, Central Iran. *Journal of Mining & Environment (JME)*, *9*(1), 209-227.

[65]. Afzal, P., Jebeli, M., Pourkermani, M., & Jafari Rad, A. (2018). Correlation between rock types and Copper

mineralization using fractal modeling in Kushk-e-Bahram deposit, Central Iran. *Geopersia*, *8*(1), 131-141.

[66]. Daya, A., & Moradi, R. (2018). Comparative analysis between concentration- number (C-N) and concentration-area (C-A) fractal models for separating anomaly from background in Siahrood 100,000 sheet, NW Iran. *Journal of Aalytical and Numerical Methods in Mining Engineering*, *8*(16), 87-94.

[67]. Shafieyan, F., & Abdideh, M. (2019). Application of concentration-area fractal method in static modeling of hydrocarbon reservoirs. *Journal of Petroleum Exploration and Production Technology*, *9*(6), 1197–1202.

[68]. Helba Hossam, A., El-Makky Ahmed, M., & Khalil Khalil, I. (2021). Application of C-N fractal model, factor analysis, and geochemical mineralization probability index (GMPI) for delineating geochemical anomalies related to Mn-Fe deposit and associated Cu mineralization in west-central Sinai, Egypt. *Geochemistry Exploration Environment Analysis*, *21*(3), 2021-2031.

[69]. Torshizian, H., Afzal, P., Rahbar, K., Yasrebi, A.B., Wetherelt, A., & Fyzollahhi, N. (2021). Application of modified wavelet and fractal modeling for detection of geochemical anomaly. *Geochemistry*, *81*(4), 125800.

[70]. Liu, C., Zhao, T., Wang, G., & Chen, D. (2024). A review of China's resources of lithium in coal seams. *Frontier Energy Research*, *12*, 1008320.

[71]. Li, C., Li, Z., Wu, T., Luo, Y., Zhao, J., Li, X., Yang, W., & Chen, X. (2021). Metallogenic Characteristics and Formation Mechanism of Naomugeng Clay-Type Lithium Deposit in Central Inner Mongolia, China. *Minerals*, *11*, 238.

[72]. Arbuzov, S.I., Finkelman, R.B., Ilyenok, S.S., Maslov, S.G., Mezhibor, A.M., & Blokhin, M.G. (2019). Forms of finding rare earth elements (La, Ce, Sm, Eu, Tb, Yb, Lu) in the coals of Northern Asia. *Chem Solid Fuels*, *1*, 3‑24 (in Russian).

[73]. Kopobayeva, A.N., Amangeldikyzy, A., Blyalova, G.G., & Srajadinkyzy, A.N. (2024). Features of rare earth elements geochemistry in coals of Central Kazakhstan. *Acta Geochim*, *43*, 876-888.

[74]. Fu, B., Xu, G., Hower, J.C., Cao, Y., Huang, Y., Liang, S., Xian, L., Luo, G., Liu, G., Hu, G., & Yao, H. (2024). Recognition and (semi-)quantitative analysis of REE-bearing minerals in coal using automated scanning electron microscopy. *International Journal of Coal Geology*, *282*, 104443.

[75]. Zhou, M., Zhao, L., Wang, X., Nechaev, V.P., French, D., Spiro, B.F., Graham, I.T., Hower, J.C, & Dai, S. (2021). Mineralogy and geochemistry of the Late Triassic coal from the Caotang mine, northeastern Sichuan Basin, China, with emphasis on the enrichment of the critical element lithium. *Ore Geology Reviews*, *139*, 104582.

[76]. Dai, S. F., Zhang, W., Ward, C.R., Seredin, V.V., Hower, J.C., Li, X., Song, W., Wang, X., Kang, H., & Zheng, L. (2013). Mineralogical and geochemical anomalies of late Permian coals from the Fusui coalfield, Guangxi Province, southern China: Influences of terrigenous materials and hydrothermal fluids. *International Journal of Coal Geology*, *105*, 60–84.

[77]. Wang, Q., Yan, Q., Zhang, Y., & Zhou, F. (2022). Enrichment Mechanism of Lithium in Late Permian Coals in the Bijie Area, Guizhou, China. *ACS Omega*, *7*(19), 16361–16370.

[78]. Lide, D.R. 2004. CRC handbook of chemistry and physics 85th edition. *CRC press*, Boca Raton, 2712.

[79]. Wang, Z., Dai, S., Zou, J., French, D., & Graham, I.T. (2019). Rare earth elements and yttrium in coal ash from the Luzhou power plant in Sichuan, Southwest China: Concentration, characterization and optimized extraction. *International Journal of Coal Geology*, *203*(2), 1-14

[80]. Jozanikohan, G., Abarghooei, M.N., & Sedighi, H. (2021). Geochemical Study of Rare Earth Elements Content in Tabas Coal Ash, Parvadeh Coal Mine. *Journal of Mining and Environment (JME)*, *12*(4), 1143-1153.

انجمن مهندسی معدن ایران
نشریه مهندسی معدن و محیط زیست
نشانی نشریه: www.jme.shahroodut.ac.ir
دانشگاه صنعتی شاهرود

استفاده از مدل‌های فرکتالی برای تعیین الگوی توزیع عناصر کمیاب و لیتیوم در کانسار زغالسنگ کوچکعلی شمالی، طبس

مجتبی بازرگانی گلشن[1]، مهران آرین[1*]، پیمان افضل[2]، لی‌لی دانشور صایین[3] و محسن آل‌علی[1]

۱. بخش علوم پایه، واحد علوم و تحقیقات، دانشگاه آزاد اسلامی، تهران، ایران
۲. بخش مهندسی نفت و معدن، واحد تهران جنوب، دانشگاه آزاد اسلامی، تهران، ایران
۳. گروه زمین شناسی، دانشگاه پیام نور، صندوق پستی ۳۶۹۷-۱۹۳۹۵، تهران، ایران

اطلاعات مقاله

تاریخ ارسال: ۲۰۲۴/۱۱/۰۹
تاریخ داوری: ۲۰۲۴/۱۱/۲۹
تاریخ پذیرش: ۲۰۲۴/۱۲/۱۲

DOI: 10.22044/jme.2024.15323.2938

کلمات کلیدی

مدل فرکتالی عیار- تعداد
مدل فرکتالی عیار- مساحت
عناصر کمیاب
لیتیوم
کوچکعلی شمالی

چکیده

هدف از این پژوهش استفاده از مدل‌های فرکتالی عیار- تعداد و عیار- مساحت به منظور تعیین الگوی توزیع عناصر کمیاب و لیتیوم در محدوده معدنی کانسار زغالسنگ کوچکعلی شمالی است. با توجه به نمودارهای فرکتالی عیار- مساحت و عیار- تعداد، چهار گروه ژئوشیمیایی متفاوت برای عناصر کمیاب و لیتیوم در محدوده معدنی کانسار زغالسنگ کوچکعلی شمالی بدست آمد. مقایسه مقادیر آستانه و مدل‌های بدست‌آمده براساس مدل‌های فرکتالی عیار- مساحت و عیار- تعداد نشان می‌دهد که مدل فرکتالی عیار- مساحت در تعیین گروه‌های ژئوشیمیایی مختلف و جداسازی ناهنجاری‌های عناصر کمیاب و لیتیوم از زمینه در کانسار زغالسنگ کوچکعلی شمالی بهتر عمل کرده است. براساس مدل‌های فرکتالی، در محدوده معدنی، بخش‌های جنوب شرقی و غربی بیشترین عیار عناصر کمیاب و بخش‌های شمال شرقی بیشترین عیار لیتیوم را دارا می‌باشد. این بخش‌های به دلیل ارزش اقتصادی بالاتر باید در عملیات معدنی مورد توجه قرار گیرند. محل ناهنجاری‌های عناصر کمیاب منطبق بر محل گسل‌های راستگرد با مولفه نرمال است، از آنجایی که این گسل‌ها جوان هستند و پس از تشکیل لایه‌های زغالسنگ عمل کرده‌اند، بنابراین کانی‌زایی عناصر کمیاب در کانسار زغالسنگ کوچکعلی شمالی اپی‌ژنتیک است.

نویسنده مسئول مکاتبات: mehranarian@yahoo.com(م. آرین)